第 49 卷第 3 期　　硅　酸　盐　学　报　　Vol. 49，No. 3
2021 年 3 月　　JOURNAL OF THE CHINESE CERAMIC SOCIETY　　March，2021
http://www.gxyb.cbpt.cnki.net　　**DOI**：10.14062/j.issn.0454-5648.20200450

1 700 ℃流动氮气下金属铝–镁铝尖晶石复合材料的物相组成与反应机理

闫明伟[1,2]，杨裕民[3]，李　勇[4]，刘开琪[1,2]，孙广超[1,2]，张佳钰[1]，胡超权[2]

(1. 中国科学院过程工程研究所多相复杂系统国家重点实验室，北京 100190；2. 中科院过程工程研究所南京绿色制造产业创新研究院，南京 211135；3. 中航天水高新磨料有限公司，甘肃 天水 741024；4. 北京科技大学材料科学工程学院，北京 100083)

摘　要：研究了高纯氮气下先后进行 580 ℃保温 8 h、1 700 ℃保温 3 h 热处理后 Al–$MgAl_2O_4$ 复合材料的物相组成和反应机理。结果表明：经 580 ℃保温 8 h 后，Al–$MgAl_2O_4$ 复合材料形成分层现象，即外层区含金属铝–氮化铝壳核结构。当温度升至某一特定值时，金属铝–氮化铝壳核结构破裂，金属铝 Al(l/g)溢出/逸出，与 N_2 和 O_2 分别反应生成 AlN 和 Al_2O(g)，促进化学计量比的镁铝尖晶石($MgAl_2O_4$)分解形成富氧化铝的镁铝尖晶石(Al_2O_3-rich spinel)和镁蒸气(Mg(g))。一方面，AlN 与富氧化铝的镁铝尖晶石形成 MgAlON 尖晶石；另一方面，AlN 与 Mg(g)和 O_2 发生固溶体反应生成氮化铝固溶体，(Mg,Al)(N,O)。内层区的材料物相组成不同于外层区，含有许多由气–气反应 $Al_2O(g)+O_2(g)+N_2(g)+Mg(g)\rightarrow MgAlON(s)$或 $Al(g)+O_2(g)+N_2(g)+Mg(g)\rightarrow MgAlON(s)$生成的片状 MgAlON；此外，内层区富氧化铝的镁铝尖晶石没有进一步转变为 MgAlON 尖晶石。

关键词：壳核结构，富氧化铝镁铝尖晶石，镁阿隆，氮化铝固溶体
中图分类号：　　**文献标志码：**A　　**文章编号：**0454–5648(2021)03–0590–07
网络出版时间：2021–01–21



Phase Composition and Reaction Mechanism of Aluminum–Spinel Composite at 1 700 ℃ in Flowing Nitrogen

YAN Mingwei[1,2], *YANG Yumin*[3], *LI Yong*[4], *LIU Kaiqi*[1,2], *SUN Guangchao*[1,2], *ZHANG Jiayu*[1], *HU Chaoquan*[2]

(1. State Key Laboratory of Multiphase Complex Systems, Institute of Process Engineering, Chinese Academy of Sciences, Beijing 100190, China; 2. Nanjing IPE Institute of Green Manufacturing Industry, Nanjing 211135, China; 3. Avic Tianshui New & High Abrasives Co., Ltd., Tianshui 741024, China; 4. School of Materials Science and Engineering, University of Science and Technology, Beijing 100083, China)

Abstract: The phase composition and reaction mechanism of aluminum-spinel (Al–$MgAl_2O_4$) composite were investigated after being treated at 580 ℃ for 8 h and 1 700 ℃ for 3 h in flowing high purity nitrogen. The results show that after being treated at 580 ℃ for 8 h, the Al–$MgAl_2O_4$ composite forms an area phenomenon with the aluminum-aluminum nitride (Al–AlN) core–shell structure in the outside area. When the temperature increases up to a critical value, the Al–AlN core–shell structure in the outside area breaks, Al(l/g) reacts with N_2 to form AlN and with O_2 to form Al_2O(g). This process prompts formation of an $MgAl_2O_4$ spinel with stoichiometric ratio that allows decomposition into Al_2O_3-rich spinel and Mg(g). On the one hand, AlN reacts with Al_2O_3-rich spinel to form MgAlON spinel, and on the other hand, AlN is transformed into (Mg,Al)(N,O) through the solid solution reaction of Mg(g) and O_2(g) into AlN. Phase composition of the inside area is different from the outside area in which MgAlON with flake crystal morphology forms *via* a gas–gas phase reaction: $Al_2O(g)+O_2(g)+N_2(g)+Mg(g)\rightarrow MgAlON(s)$ or $Al(g)+O_2(g)+N_2(g)+Mg(g)\rightarrow MgAlON(s)$ in which Al_2O_3-rich spinel doesn't further form MgAlON spinel.

Keywords: core–shell structure; aluminum oxide–rich spinel; magnesium aluminum oxynitride; aluminum nitride solid solution

收稿日期：2020–06–22。　修订日期：2020–07–11。
基金项目：中科院过程工程研究所南京绿色制造产业创新研究院关键研究项目(E0010717)。
第一作者：闫明伟(1989—)，男，博士后。
通信作者：刘开琪(1969—)，男，研究员。

Received date: 2020–06–22.　**Revised date:** 2020–07–11.
First author: YAN Mingwei (1989–), male, Postdoctor.
E-mail: mwyan@ipe.ac.cn
Corresponding author: LIU Kaiqi (1969–), male, Professor.
E-mail: kqliu@ipe.ac.cn

1 Introduction

Magnesium aluminium oxynitride (MgAlON) has been widely studied as a promising superior refractory compound due to high compressive and high flexural strengths, high resistance to slag and metal attack, and low thermal expansion coefficient (5.3×10^{-6} K^{-1}–7.4×10^{-6} K^{-1})[1–6]. MgAlON is a type of solid solution ceramic with the same crystal structure as AlON and magnesium aluminate ($MgAl_2O_4$) spinels[7]. Its crystal structure formulation is described below: $Mg_yAl_{3-y-(1/3)x}\square_{(2/3)x}O_{3+x+y}N_{1-x-y}$ ($0\leqslant x\leqslant 1$; $\leqslant y\leqslant 1$; $x+y\leqslant 1$; $\square$ represents vacancy)[8], and the relationship between crystal lattice constant and composition fulfills the formula: a=0.790+0.037 5 [MgO, mole fraction]+0.015 [AlN, mole fraction]/(nm)[9]. Because of non-oxide oxidation susceptibility, MgAlON is unstable and easily decomposes into an Al_2O_3-rich spinel and Al_2O_3, thus releasing nitrogen at high temperatures into the air[10]. Both aluminum oxide (Al_2O_3) and Al_2O_3-rich spinels present high melting points. Al_2O_3-rich spinels can accommodate some oxides, such as iron, manganese, and magnesium oxides (FeO, MnO, and MgO, respectively) and Al_2O_3 as spinel solid solutions. After nitrogen enters the slag, the viscosity of the slag increases, which further enhances slag penetration resistance of MgAlON bonded refractories[11–12].

MgAlON can be produced in several ways: (1) carbothermal reaction and nitridation[13], (2) solid state reaction[14–21], and (3) aluminothermy nitridation reaction[22–23]. The aluminothermy nitridation and solid state reactions. as the main methods, are used to prepare MgAlON-bonded Al_2O_3 and MgO-based refractory refractories[20–23]. The formation mechanism of a MgAlON spinel *via* the solid state reaction has been investigated by Granon et al. and Weiss et al.[8–9] based on the analysis of AlN–Al_2O_3–MgO ternary system phase diagrams and can be described as proceeding *via* two steps: (1) MgO reacts with Al_2O_3 to form Al_2O_3-rich spinel above 1 000 ℃ and (2) AlN and Al_2O_3 dissolve into the Al_2O_3-rich spinel to form a MgAlON spinel at high temperatures. The maximal amount AlN and Al_2O_3 that dissolves into Al_2O_3-rich spinel increases with an increase in the heating temperature, and the diffusion rate of N element controls the rate of MgAlON formation. However, aluminothermy nitridation reaction for preparing MgAlON bonded refractories is more complex than the solid state reaction due to high metallic Al activity. Previous studies have reported the preparation and formation mechanism of MgAlON-bonded Al_2O_3-based refractories at 1 700 to 1 800 ℃ under N_2-flow using aluminum, alumina, and magnesium oxide as raw materials in addition to $MgAl_2O_4$ sol as a binding agent[19, 23]. The results show that MgAlON presents two different morphologies: flake from a gas–gas reaction and particle from solid solid reaction. The formation reaction of MgAlON is affected by the reaction of MgO and Al_2O_3 to form $MgAl_2O_4$.

After studying the corrosion behavior of Al–MgO–$MgAl_2O_4$ refractory materials, Tong et al. found that the $MgAl_2O_4$ spinel could effectively prevent the infiltration of calcium oxide-silicon dioxide (CaO–SiO_2)-based slag by reacting with AlN to form MgAlON[24]. Therefore, it is necessary to investigate phase compositions and reaction mechanisms of Al–MgO and Al–$MgAl_2O_4$ composites, which involves industrial application of MgAlON-bonded refractory materials at high temperatures during the process of steel melting. Studies on phase composition and reaction mechanisms of Al–MgO composite have been well investigated by Sun et al.[25] in which a MgAlON spinel could be formed by the reactions of 2Al(l)+4MgO(s)→$MgAl_2O_4$+3Mg(g) and Al(l)+0.5N_2(g)→AlN and $MgAl_2O_4$+AlN→MgAlON. In this current study, research on investigating phase composition and reaction mechanisms of the Al–$MgAl_2O_4$ composite was conducted in flowing nitrogen using the aluminothermy nitridation method with Al and $MgAl_2O_4$ with stoichiometric ratio as raw materials. It was expected to provide some basic theoretical data for industrial applications of MgAlON-bonded refractories.

2 Experimental

The $MgAl_2O_4$ spinel with stoichiometric ratio (Taimei Chemicals Co., Ltd., Japan $w(MgAl_2O_4)\geqslant$ 99.99%, partical size<44 μm) and metal Al (Luoyang Discover Aluminium Co., Ltd., China w(Al)>99.2%, partical size<44 μm) were used as raw materials. The starting powders were mixed by ball milling in an alcohol liquid using a planetary ball mill. The mass ratio of $MgAl_2O_4$:Al was fixed at 70:30. Following ball milling at 500 r/min for 30 min, the slurry with a particle size of D_{50}=24 μm was dried in air and pressed into one sample with dimensions of ϕ15 mm×25 mm under a pressure of 10 MPa. The sample was then named as the A–$MgAl_2O_4$ composite and placed into a carbon tube furnace and treated at 580 ℃ for 8 h and 1 700 ℃ for 3 h under flowing nitrogen (0.101 MPa, N_2 99.999%, O_2 0.001%). Heat treatment at 580 ℃ for 8 h was done to form an Al–AlN core-shell structure[12]. Fig. 1 shows the X-ray diffraction (XRD) pattern of $MgAl_2O_4$ spinel with stoichiometric ratios. According to PDF card (COD96-900-5769), we could determine its crystal lattice constant with a=b=c= 0.808 8 nm, and the relationship with MgO: Al_2O_3=1:1 in the selected $MgAl_2O_4$ spinel is also acquired based on the formula shown below: $a_{MgAl_2O_4}$=0.790+ 0.037 5x_{MgO} nm[8].

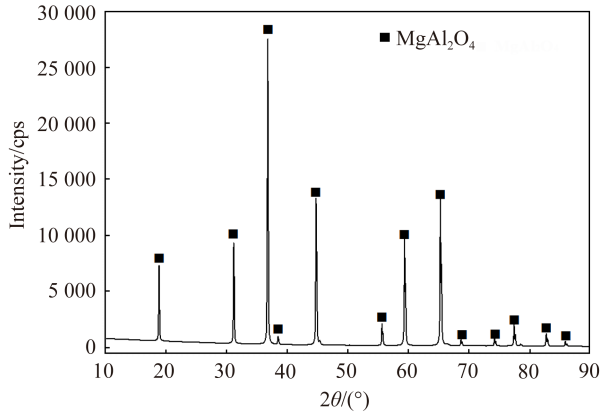


Fig. 1 XRD pattern of a magnesium aluminate ($MgAl_2O_4$) spinel with stoichiometric ratios

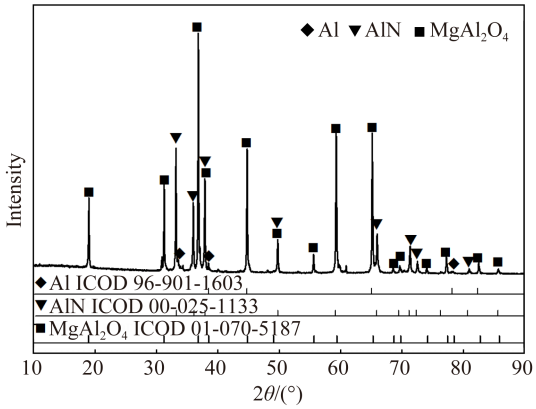


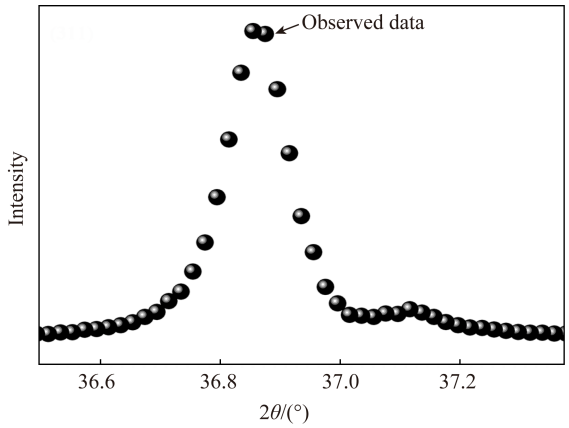
Fig. 2 XRD pattern of the Al–$MgAl_2O_4$ composite after being treated at 580 ℃ for 8 h and 1 700 ℃ for 3 h under flowing nitrogen

The phase composition of the Al–$MgAl_2O_4$ composite after being treated at 1 700 ℃ under flowing nitrogen was characterized with an X-ray diffractometer (D8 ADVANCE, Germany) with a scanning time of 10 min and 2θ range of 10° to 90°. The microstructure of the Al–$MgAl_2O_4$ composite was investigated with a scanning electron microscope ([SEM] Quanta200, FEI, Holland) equipped with an energy dispersive spectroscope ([EDS] INCA250 Oxford Instrument, UK).

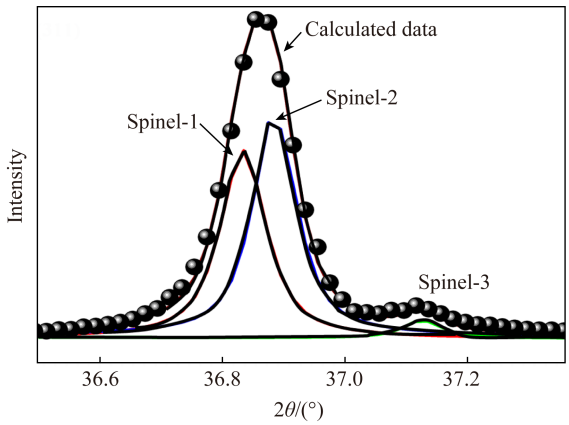
3 Results and discussion

3.1 Characterization and analysis of phase composition

Fig. 2 shows the XRD pattern of the Al–$MgAl_2O_4$ composite after being treated at 1 700 ℃ under flowing nitrogen. It can be seen that the diffraction characteristic peaks of the Al–$MgAl_2O_4$ composite are consistent with those of $MgAl_2O_4$ spinel, AlN, and Al according to the *HighScore Plus* analysis software. After the strongest diffraction peak (311) of spinel phase in the Al–$MgAl_2O_4$ composite was identified, it was further treated for peak processing by means of XPSPEAK software. As shown in Fig. 3, it can be seen in Fig. 3 that the Al–$MgAl_2O_4$ composite presents three types of spinels, Spinels–1–3, and their corresponding interplanar spacings, d, were 0.243 8, 0.243 6, and 0.242 0 nm, respectively. According to the relationship among the crystal lattice constant a, interplanar spacing d, and crystal indices (hkl): $d=\frac{a}{\sqrt{h^2+k^2+l^2}}$, the crystal lattice constants of Spinels-1–3 were 0.808 6, 0.807 9, and 0.802 6 nm, respectively, which was less than that of the $MgAl_2O_4$ spinel with stoichiometric ratio. It indicates that the $MgAl_2O_4$ spinel with stoichiometric ratio is transformed into the three spinel types with different crystal lattice constants after being treated at 580 ℃ for 8 h and 1 700 ℃ for 3 h.



(a) Original data



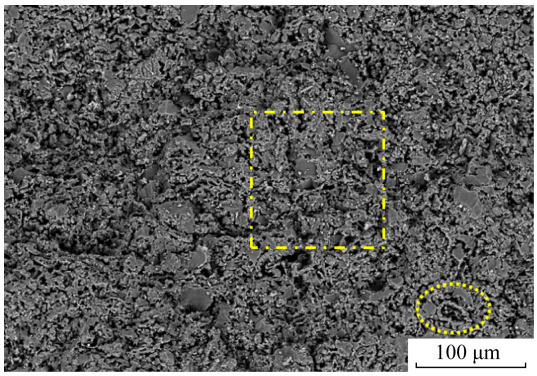
(b) Treated data

Fig. 3 XRD pattern of the strongest diffraction peak (311) of spinel phase shown in Fig. 2

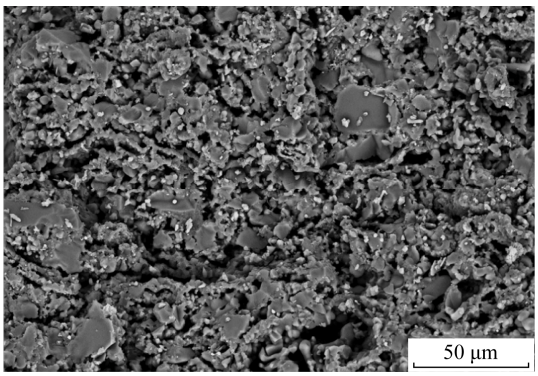
3.2 Characterization and analysis of organization structure

The Al–$MgAl_2O_4$ composite presented two obvious areas after being treated at 580 ℃ for 8 h and 1 700 ℃ for 3 h under flowing nitrogen: an compact outside area and and inside loose inside area. Fig. 4

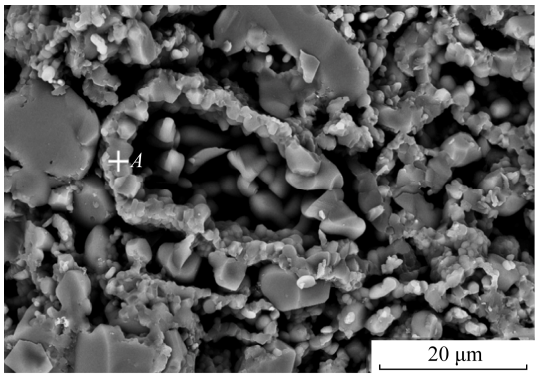
shows SEM images of the compact outside area. As observed, the compact outside area has good sintering characteristics. Based on the analysis results from Table 1, some conclusions could be drawn in which the $MgAl_2O_4$ spinel with stoichiometric ratio was transformed into spinel consisting of Mg, Al, O, and N, and AlN existed in the form of AlN solid solution (Mg, Al)(O,N). The results above illustrate that after Al–AlN core–shell structure broke, the partial oxygen pressure in the Al–$MgAl_2O_4$ composite greatly decreased, and the $MgAl_2O_4$ spinel with stoichiometric ratio decomposed into an Al_2O_3-rich spinel and Mg(g) to result in the formation of a MgAlON spinel through the diffusion reaction of AlN into the Al_2O_3-rich spinel.



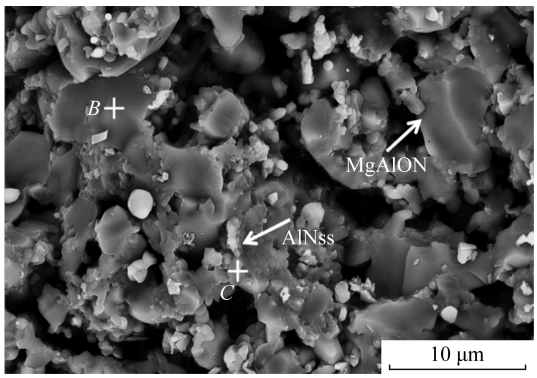
(a) SEM photograph with low magnification



(b) SEM photograph of the square area in Fig. 4(a)



(c) SEM photograph of the elliptical area in Fig. 4(a)



(d) SEM photograph with high magnification

Fig. 4　SEM photographs of the compact outside area in the Al–$MgAl_2O_4$ composite after being treated at 580 ℃ for 8 h and 1 700 ℃ for 3 h

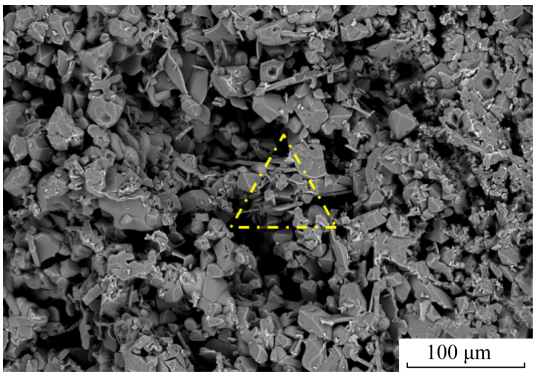
Table 1　Energy-dispersive EDS analysis results of the selected areas in Fig. 4

Area	Atom fraction/%			
	Mg	Al	O	N
A	2.2	46.3	7.2	44.3
B	17.1	39.7	38.3	4.9
C	3.4	46.5	7.5	42.6

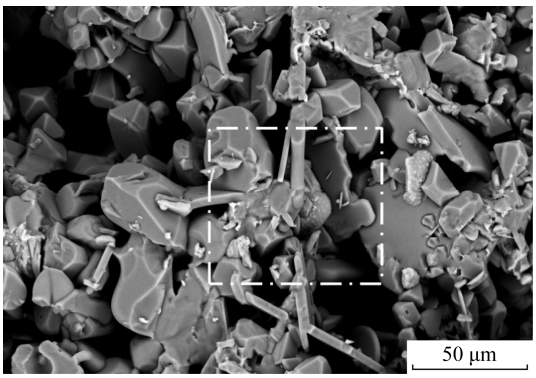
Fig. 5 shows SEM images of the loose inside area in the Al–$MgAl_2O_4$ composite. Different from the phase composition and organizational structure of the compact outside area, the loose inside area had an inferior sintering characteristic, its organizational structure was relatively loose, and many flake crystals were found. Some information can be acquired from Table 2. The flake crystal consists of the MgAlON spinel phase, and its N content was more than that of MgAlON in the compact outside area; the Al_2O_3-rich spinel from the $MgAl_2O_4$ spinel with stoichiometric ratio did not transform into MgAlON spinel, and AlN crystallized from liquid Al. Based on the analysis of phase composition and organizational structure of the compact outside area and the loose inside area, the Al–$MgAl_2O_4$ composite presented two areas with different phase composition and phase evolution processes at high temperatures after being treated at 580 ℃ for 8 h. This process occurred because of the limited nitrogen infiltration capacity from the outside to the inside area. According to the energy-dispersive EDS analysis results from Tables 1 and 2, it can be concluded that Spinels–1–3 consisted of the the Al_2O_3-spinel of the loose inside area, MgAlON spinel of the compact outside area, and flake MgAlON of the inside loose inside area, respectively.

3.3　Discussion and analysis

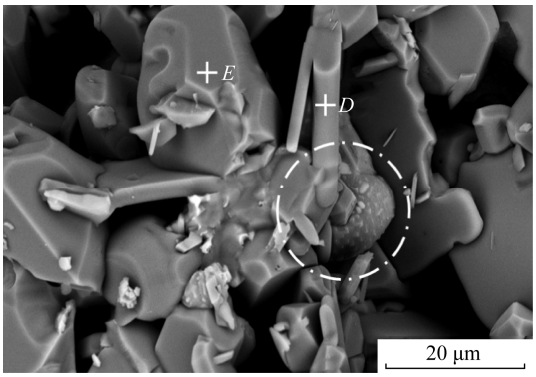
According to Kelvin's equation, curved liquid surfaces possess a saturated vapor pressure much greater than that of flat liquid surfaces. Saturated



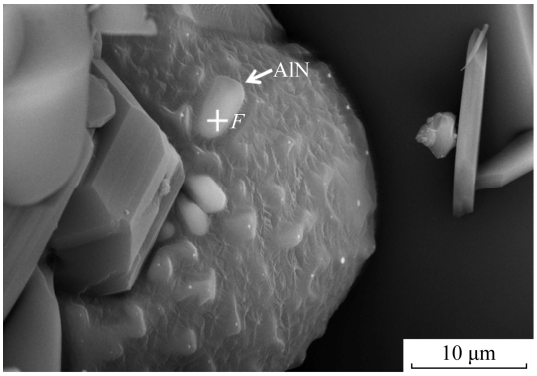
(a) SEM photograph with low magnification



(b) SEM photograph of the triangular region in Fig. 5(a)



(c) SEM photograph of the square area in Fig. 5(b)



(d) SEM photograph of the round area in Fig. 5(c)

Fig. 5 SEM photographs of the loose inside area in the A–$MgAl_2O_4$ composite after being treated at 580 ℃ for 8 h and 1 700 ℃ for 3 h

Table 2 EDS analysis results of the selected areas in Fig. 5

Area	Atom fraction/%			
	Mg	Al	O	N
D	8.8	54.8	13.5	22.9
E	13.3	30.0	56.7	—
F	0.8	51.7	3.2	44.3

vapor pressures of curved liquid surfaces can be described as shown in the following equation:

$$\ln\frac{P}{P_0}=\frac{2\sigma M}{\rho RT}\cdot\frac{1}{r} \tag{1}$$

in which ρ, M and R are density, molecular mass, and gas constant of liquid, respectively; P is the saturated vapor pressure of the curved liquid surface, P_0 is saturated vapour pressure of flat liquid surface; r is radius of spherical liquid drop, and σ is liquid surface tension. For liquid Al with a size of 44 μm in diameter, the relationship between saturated vapor pressure of curved liquid surface and saturated vapor pressure of flat liquid surface can be given as $P=\mathrm{e}^{\frac{2\sigma M}{\rho RT}}\cdot\mathrm{e}^{\frac{10^6}{12}}P_0>\mathrm{e}^{\frac{10^6}{12}}P_0$. This finding indicates that the saturated vapor pressure of Al with curved liquid surface was much higher than that of its flat liquid surface.

Therefore, when the temperature increased to a critical value, the Al–AlN core-shell structure breaks due to phase transformation volume effects and liquid Al(l) is transformed into gas Al(g). Driven by powerful saturated vapor pressure, Al(g) diffused and transferred along pores or gaps in the outer area of the Al–$MgAl_2O_4$ composite. On the one hand, Al(g) reacted with O_2 to form Al_2O(g), resulting in a drastic reduction in partial oxygen pressure in the Al–$MgAl_2O_4$ composite; on the other hand, Al(l/g) reacted with N_2 to form AlN. As a result, different phase composition and phase evolution processes happened in the outer and the inside areas of the Al–$MgAl_2O_4$ composite at high temperatures.

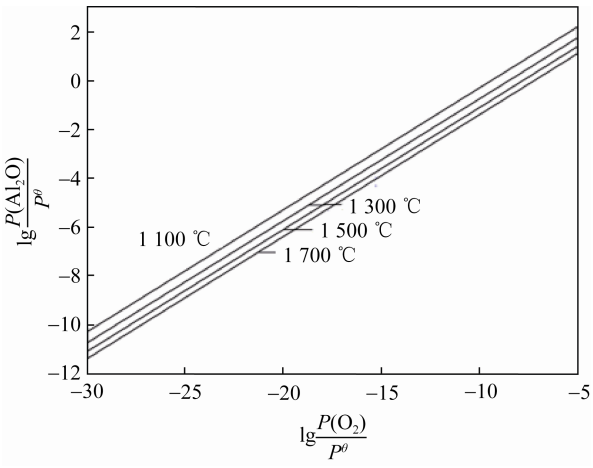
3.3.1 Phase evolution of the outside area

Due to the consuming oxygen reaction, $2Al(l/g)+0.5O_2\rightarrow Al_2O(g)$, when partial oxygen pressure was reduced to a critical value, the $MgAl_2O_4$ spinel with stoichiometric ratio would decompose into an Al_2O_3-rich spinel according to the reaction $MgAl_2O_4(s)\rightarrow Al_2O_3$-rich spinel+$Mg(g)+O_2(g)$. The Al_2O_3-rich spinel contained a higher proportion of tetrahedron and octahedron vacancies than the $MgAl_2O_4$ spinel with stoichiometric ratio, which could have provided a favorable diffusion passageway for anionic N. Therefore, AlN generated by the Al(l/g) –N_2 reaction would diffuse into the Al_2O_3-rich spinel to form MgAlON spinel at high temperatures based on the reaction: Al_2O_3-rich spinel+$AlN(s)\rightarrow MgAlON(s)$. Mg^{2+} (0.049 nm), Al^{3+} (0.039 nm), O^{2-} (0.140 nm), and N^{3-} (0.171 nm) meet the relationship formula: $15\%<\Delta<30\%$ (Δ represents the change ratio of relative

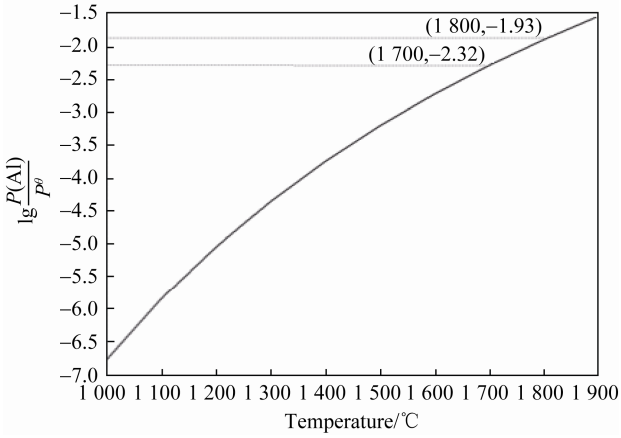
radius, $\Delta=\left|\frac{r_1-r_2}{r_1}\right|\times100\%$)[26], which leads to the finding that Mg and O elements easily entered into the AlN crystal lattice and existed as AlN solid solution ((Mg,Al)(O,N)) according to the reaction $2Mg+O_2 \xrightarrow{AlN} 2Mg'_{Al}+2O^{\times}_{N}$ ("′" and "×" represent for a negative and a positive charge respectively). According to the analysis results from Figs. 1 and 3 in which the $MgAl_2O_4$ spinel with stoichiometric ratio was transformed into an MgAlON spinel, and AlN was transformed into (Mg,Al)(O,N), the above calculation above appears to be correct. In addition, the grain boundary between (Mg, Al)(O,N) and MgAlON partially merges to endow the outside area with good sintering characteristics.

3.3.2　Phase evolution of the inside area

The partial oxygen pressure under flowing nitrogen was $\lg\frac{P(O_2)}{P^{\theta}}=-5$ in this work. Therefore, when the Al–AlN core–shell structure in the outside area did not break, gaseous products from the Al(l)–O_2(g) reaction in Al−$MgAl_2O_4$ composite were mainly composed of Al_2O(g) with trace amount of Al(g) according to Fig.6, which led to the gas–gas formation reaction of AlN in the inside area in small or negligible amounts. In the meantime, AlN began to form in liquid Al *via* the gas–liquid reaction pathway and grew increasingly larger with the increase in temperature. When Al–AlN core–shell structure breaks in the outside area, Al(l/g) reacts with N_2 to form AlN and with O_2 to form Al_2O(g), which greatly reduced the partial nitrogen and oxygen pressures to further suppress the formation reaction of AlN in the inside area due to limited nitrogen infiltration capacity and sintering effects. This process can be verified by SEM analysis results in Fig. 5 in which AlN only crystallized in liquid Al, and the Al_2O_3-rich spinel was not transformed into MgAlON spinel. Therefore, when the temperature rose to a critical value, the $MgAl_2O_4$ spinel with stoichiometric ratio decomposed into an Al_2O_3-rich spinel based on the reaction $MgAl_2O_4(s)\rightarrow Al_2O_3$-rich spinel+Mg(g)+$O_2$(g). In addition, the Al_2O_3-rich spinel could not be transformed into MgAlON because of the inexistence of AlN on its surface. Al_2O(g) from Al(g)–O_2 and Al(g) reacted with Mg(g), N_2, and O_2 to form MgAlON with a flake morphology due to its crystal-preferred growth based on the reaction: $Al_2O(g)+O_2(g)+N_2(g)+Mg(g)\rightarrow$ MgAlON(s) or $Al(g)+O_2(g)+N_2(g)+Mg(g)\rightarrow$MgAlON(s).



(a) $\lg\frac{P(Al_2O)}{P^{\theta}}$ *vs* $\lg\frac{P(O_2)}{P^{\theta}}$



(b) $\lg\frac{P(Al)}{P^{\theta}}$ *vs* T

Fig. 6　Relationship diagram of $\lg\frac{P(Al_2O)}{P^{\theta}}$ *vs* $\lg\frac{P(O_2)}{P^{\theta}}$ and $\lg\frac{P(Al)}{P^{\theta}}$ *vs* T[23, 27–28]

4　Conclusions

1) After treatment at 580 ℃ for 8 h and 1 700 ℃ for 3 h, the Al–$MgAl_2O_4$ composite formed an area phenomenon with Al–AlN core–shell structure in the outside layer due to the limits of the nitrogen infiltration capacity and sintering effects.

2) When the temperature increased to a critical value, the Al–AlN core–shell structure in the outside area broke, and Al(l/g) reacted with N_2 to form AlN and with O_2 to form Al_2O(g), which prompted $MgAl_2O_4$ with stoichiometric ratio to decompose into an Al_2O_3-rich spinel and Mg(g). Al_2O_3-rich spinel then reacted with AlN to form MgAlON spinel, and AlN was transformed into the AlN solid solution (Mg,Al)(N,O).

3) The phase composition of the inside area is different from the outer layer in which MgAlON with flake crystal morphology was formed via the gas–gas phase reaction: $Al_2O(g)+O_2(g)+N_2(g)+$ $Mg(g)\rightarrow$MgAlON(s) or $Al(g)+O_2(g)+N_2(g)+Mg(g)\rightarrow$

MgAlON(s), and the Al_2O_3-rich spinel did not further form MgAlON spinel.

References:

[1] DENG C J, HONG Y R, ZHONG X C, et al. Slag-resistance of MgAlON spinel[J]. J Univ Sci Technol Beijing, 2000, 7(2): 96–98.

[2] BANDYOPADHYAY S, RIXECKER G, ALDINGER, et al. Effect of controlling parameters on the reaction sequences of formation of nitrogen containing magnesium aluminate spinel from MgO, Al_2O_3, and AlN[J]. J Am Ceram Soc, 2004, 87(3): 480–482.

[3] ZHANG Z, TENG L, LI W. Mechanical properties and microstructures of hot-pressed MgAlON–BN composites[J]. J Eur Ceram Soc, 2007, 27(1): 319–326.

[4] ZHANG Z T, MATSUSHITA W C, LI S, et al. Reactions between MgAlON–BN composites and CaO–SiO_2–Al_2O_3–MgO–FeO slag[J]. Metall Mater Trans B, 2007, 38(2): 231–241.

[5] ZHANG H X, ZHANG Y R, HONG Y, et al. Precise determination of the MgAlON/(AlN+MgAlON) phase boundaries in the MgO–AlN–Al_2O_3 ternary system at 1 600 ℃ and 1 700 ℃[J]. J Mater Sci Tech, 2005, 21(2): 277–280.

[6] PICHLBAUER S, HARMUTH H, Z.LENCES Z, et al. Preliminary investigations of the production of MgAlON bonded refractories[J]. J Euro Ceram Soc, 2012, 32(9): 2013–2018.

[7] WANG X D, WANF F M, LIU W C. Synthesis thermodynamics and properties of MgAlON[J]. J Inorg Mater, 2003, 18(1): 83–90.

[8] WEISS S, GREIL PGAUCKLER L J. The system A1–Mg–O–N[J]. J Am Ceram Soc, 1982, 65(5): 68–69.

[9] GRANON A, GOEURIAT P, THEVENOT J, et al. Reactivity in the Al_2O_3–AlN–MgO system. The MgAlON spinel phase[J]. J Eur Ceram Soc, 1994, 13(4): 365–370.

[10] DAI W B, YAMAGUCHI A, LIN W, et al. Oxidation behavior of magnesium aluminum oxynitride with different composition[J]. J Ceram Soc Jpn, 2007, 115(1339): 409–413.

[11] DIAZ L A, TORRECILLAS A H, PNEA P, et al. Effect of spinel content on slag attack resistance of high alumina refractory castables[J]. J Eur Ceram Soc, 2007, 27(16): 4623–4631.

[12] YAN M W, LI Y, LI H Y, et al. Preparation and ladle slag resistance mechanism of MgAlON bonded Al_2O_3–MgAlON–$Zr_2Al_3C_4$–$(Al_2CO)_{1-x}(AlN)_x$ refractories[J]. Ceram Int, 2019, 45(1): 346–353.

[13] DAI W B, LIN W, YAMAGUCHI A, et al. Synthesis of magnesium aluminum oxynitride by carbothermal reduction and nitridation process[J]. J Ceram Soc Jpn, 2007, 115(1337): 42–46.

[14] ZHANG H X, HONG Y R, HUANG J L, et al. Precise determination of the MgAlON/(AlN + MgAlON) phase boundaries in the MgO–AlN–Al_2O_3 ternary system at 1 600 ℃ and 1 700 ℃[J]. J Mater Sci Tech, 2005, 21(2): 277–280.

[15] ZHANG Z T, MATSUSHITA T, LI W C, et al. Investigation of wetting characteristics of liquid iron on dense MgAlON-based ceramics by X-Ray sessile drop technique[J]. Metall Mater Trans B, 2006, 37(3): 421–429.

[16] BANDYOPADHYAY S, RIXECKERF, ALDINGER F, et al. Effect of controlling parameters on the reaction sequences of formation of nitrogen containing magnesium aluminate spinel from MgO, Al_2O_3, and AlN[J]. J Am Ceram Soc, 2004, 87(3): 480–502.

[17] DAI W B, YAMAGUCHI W B, LIN W, et al. Preparation and properties of spark plasma sintered magnesium aluminum oxynitride[J]. J Ceram Soc Jpn, 2007, 115(1345): 525–529.

[18] LIU X, WANG H, TU B T, et al. Highly transparent $Mg_{0.27}Al_{2.58}O_{3.73}N_{0.27}$ ceramic prepared by pressureless sintering[J]. J Am Ceram Soc, 2014, 97(1): 63–66

[19] YAN M W, LI Y, SUN J L, et al. Sun. *In-situ* synthesis and reaction mechanism of MgAlON in Al_2O_3–MgO composites produced in flowing nitrogen[J]. Ceram Int, 2017, 43(17): 14791–14797.

[20] GSCHIEL S, HARMUTH H, LENCES Z, et al. Production of MgAlON bonded alumina refractories[J]. Interceram Int Ceram Review, 2012, 1(1): 48–51.

[21] PICHLBAUERA S, HARMUTH H, LENCES Z, et al. Preliminary investigations of the production of MgAlON bonded refractories[J]. J Euro Ceram Soc, 2012, 32(9): 2013–2018.

[22] TONG S H, LI Y, YAN M W, et al. *In situ* reaction mechanism of MgAlON in Al–Al_2O_3–MgO composites at 1 700 ℃ under flowing N_2[J]. Int J Min Met Mater, 2017, 24(9): 1061–1066.

[23] YAN M W, LI Y, LI H Y, et al. Evolution mechanism of MgAlON in the Al–Al_2O_3–MgO composite at 1 800 ℃ in flowing nitrogen[J]. Ceram Int, 2018, 44(4): 3856–3861.

[24] TONG S H, ZHAO J Z, ZHANG Y C, et al. Corrosion mechanism of Al–MgO–$MgAl_2O_4$ refractories in RH refining furnace during production of rail steel[J]. Ceram Int, 2020, 46(8): 10089–10095.

[25] SUN Y, CHEN S J, TIAN L, et al. Formation of MgAlON in MgO–Al composites obtained by carbon embedded firing[J]. Naihuo Cailiao (in Chinese), 2016, 5(6): 428–430.

[26] YAN M W, LI Y, SUN Y, et al. Controllable preparation and synthetic mechanism of mullite from the bauxite with Fe-rich oxide content[J]. Mater Chem Phys, 2017, 202(1): 245–250.

[27] CHEN Z Y. Chemical Thermodynamics of Refractories[M]. Beijing: Metallurgical Industry Press; 2001: 420–421, 648.

[28] CHASE J R M W. NIST–JANAF Thermochemical Tables, 4th edition[M]. Washington DC: American Chemical Society and the American Institute of Physics for the National Institute of Standards and Technology, 1998: 1–1856.